

Finite-element Simulation of Seismic Ground Motion with a Voxel Mesh

KAZUKI KOKETSU¹, HIROYUKI FUJIWARA², and YASUSHI Ikegami³

Abstract—Accurate simulation of seismic ground motion for three-dimensionally complex topography and structures is one of the most important goals of strong motion seismology. The finite-element method (FEM) is well suited for this kind of simulation, since traction-free conditions are already included in the formulation, and the Courant condition is less strict than for the finite-difference method (FDM). However, the FEM usually requires both large memory and computation time. These limitations can be overcome by using a mesh consisting of voxels (rectangular prisms) with isotropy built into the explicit formulation of the dynamic matrix equation. Since operators in the voxel FEM are the combinations of ordinary FDM operators and additional terms, the method keeps accuracy of the same order as FDM and the terms relax the Courant condition. The voxel FEM requires a similar amount of memory and only takes 1.2 ~ 1.4 times longer computation time. The voxel mesh can be generated considerably faster than the popular tetrahedral mesh. Both ground motions and static displacements due to a point or line source can be calculated using the voxel FEM approach. Comparisons with the reflectivity method and theoretical solutions demonstrate the successful implementation of the method, which is then applied to more complex problems.

Key words: Finite-element method, seismic ground motion, voxel mesh.

Introduction

Accurate simulation of seismic ground motion for three-dimensionally complex topography and structures (sedimentary basin, fault zone, subduction zone, *etc.*) is one of the most important goals of strong motion seismology. In this field, the finite-difference method (FDM: *e.g.*, OLSEN *et al.*, 1995; GRAVES, 1996; FURUMURA *et al.*, 1998) has been more popular for many years than the finite-element method (FEM: *e.g.*, BAO *et al.*, 1998; KOMATITSCH and VILOTTE, 1998), though FEM has inherent advantages over FDM as follows: (1) FEM solutions satisfy the free-surface condition directly, since the basic equations of the FEM are derived using the

¹ Earthquake Research Institute, University of Tokyo, 1-1-1 Yayoi, Bunkyo-ku, Tokyo 113-0032, Japan. E-mail: koketsu@eri.u-tokyo.ac.jp

² National Research Institute for Earth Science and Disaster Prevention, 3-1 Tennodai, Tsukuba, Ibaraki 305-0006, Japan.

³ CRC Solutions Corp., 2-7-5 Minamisuna, Koto-ku, Tokyo 136-8581, Japan.

traction-free condition at the outer boundary of a medium. (2) The Courant condition for time integration is less strict than FDM because of additional accuracy of the FEM discretization. (3) FEM can handle very complex structures with high accuracy using elements with various shapes.

As a reason for the popularity of FDM, it can be thought that FDM usually requires much less computer memory and a shorter computation time than FEM. In addition, the pre-process of FEM, *i.e.*, mesh generation, can be very time-consuming. For example, BAO *et al.* (1998) carried out an explicit FEM simulation with 13 million nodes in the San Fernando valley requiring 16 GB memory and 7.2 hours (16,667 steps) on 256 processors of Cray T3D. The mesh generation required 7.7 GB memory and spent 13 hours on a DEC 8400. On the hand, OLSEN *et al.* (1995) carried out a FDM simulation with 23 million nodes in the Los Angeles region using 2 GB memory and 23 hours (about 5,000 steps) on 512 processors of nCUBE 2. A Cray T3D with 256 processors is thirty times faster than an nCUBE 2 with 512 processors (TOP500, 1994), and so this computation time corresponds to only 2.6 hours for 16,667 steps on a Cray T3D, though the Los Angeles mesh includes almost twice more nodes than the San Fernando valley mesh.

In order to overcome these limitations of the FEM, we introduce a mesh consisting of voxels and derive an explicit formulation of the dynamic matrix equation assuming isotropic media. 'Voxel' is a term in computer graphics derived from an abbreviation of 'volume pixel.' It is actually a hexahedron or rectangular prism in three dimensions (3-D) and its cross section forms a pixel in two dimensions (2-D). The voxel mesh can be generated as easily as in FDM and reduces the complexity of the FEM formulation as already shown in engineering applications (*e.g.*, VAN RIETBERGEN *et al.*, 1996). We lose the flexibility of element shape, so that the third advantage of FEM is lessened to some extent in this voxel FEM approach. However, the voxel formulation still achieves accuracy of a similar order to that of FDM keeping the advantages (1) and (2).

We will present here a voxel-mesh approach to the finite-element simulation of seismic wave propagation and ground motions. The efficiency of this approach will be shown by comparing its results with those by FDM or semi-analytical methods.

FEM Formulation

The displacement u_i and stresses τ_{ij} due to a body force f_i in an elastic medium V of density ρ are governed by the equation of motion

$$\rho \frac{\partial^2 u_i}{\partial t^2} = \frac{\partial \tau_{ij}}{\partial x_j} + f_i \quad (1)$$

in Cartesian coordinates $(x_j) = \mathbf{x}$. If the outer boundary S of V is a free surface so that the surface traction T_i vanishes (Fig. 1), the weak form of this equation is given by

$$\int u'_i \rho \frac{\partial^2 u_i}{\partial t^2} dV + \int \frac{\partial u'_i}{\partial x_j} C_{ijkl} \frac{\partial u_k}{\partial x_l} dV = \int u'_i f_i dV, \quad (2)$$

where u'_i is a trial function and C_{ijkl} are elastic moduli of V .

We introduce a mesh with nodes at \mathbf{x}^k into the medium V and assume that we can represent u_i at the position \mathbf{x} by

$$u_i(\mathbf{x}) = \sum_k N^k(\mathbf{x}) u_i^k \quad (3)$$

using the shape functions N^k . If N^k interpolates the displacement in a finite element of V between nodes, u_i^k now stands for the displacement of the node at \mathbf{x}^k . We then adopt N^k for the trial functions u'_i following the Galerkin approach to the method of weighted residuals, so that Equation (2) is discretized as

$$\mathbf{M} \frac{d^2 \boldsymbol{\delta}}{dt^2} + \mathbf{K} \boldsymbol{\delta} = \mathbf{f}, \quad (4)$$

where $\boldsymbol{\delta}$ is the displacement vector consisting of u_i^k and \mathbf{f} is the effective force vector. The mass matrix \mathbf{M} and stiffness matrix \mathbf{K} are given by

$$\mathbf{M} = \int \mathbf{N}^T \rho \mathbf{N} dV \quad \mathbf{K} = \int \mathbf{B}^T \mathbf{D} \mathbf{B} dV. \quad (5)$$

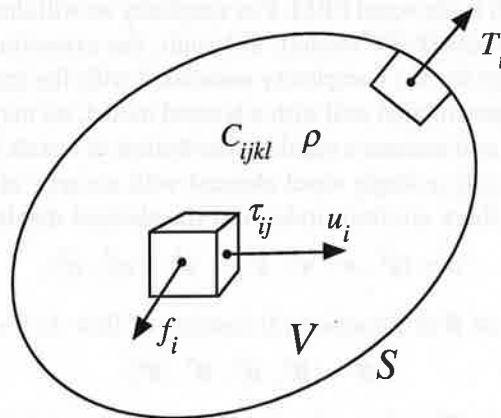


Figure 1

Displacement u_i and stresses τ_{ij} due to a body force f_i in an elastic medium V of density ρ and moduli C_{ijkl} . Surface traction T_i acts on the outer boundary S of V (after UDIAS, 1999).

The matrices \mathbf{D} , \mathbf{N} and \mathbf{B} are built from C_{ijkl} , N^k and the derivatives of N^k , respectively. In the case of an attenuative medium, a term including $d\delta/dt$ is introduced into the matrix equation (4) as

$$\mathbf{M} \frac{d^2\delta}{dt^2} + \mathbf{C} \frac{d\delta}{dt} + \mathbf{K}\delta = \mathbf{f}, \quad (6)$$

where \mathbf{C} is the damping matrix associated with the attenuation.

Substituting the second-order central differences for $d^2\delta/dt^2$ and backward differences for $d\delta/dt$, we obtain the explicit FEM formulation

$$\mathbf{M} \frac{\delta_{t+\Delta t} - 2\delta_t + \delta_{t-\Delta t}}{(\Delta t)^2} + \mathbf{C} \frac{\delta_t - \delta_{t-\Delta t}}{\Delta t} + \mathbf{K}\delta_t = \mathbf{f}_t \quad (7)$$

where $\delta_t = \delta(t)$ and $\mathbf{f}_t = \mathbf{f}(t)$.

We use the lumped mass approximation to \mathbf{M} , which amounts to lumping the mass of a finite element on its vertices as $\rho(\mathbf{x}) = \sum \rho^k \delta(\mathbf{x} - \mathbf{x}^k)$. This results in the diagonalization of \mathbf{M} , so that the matrix inversion \mathbf{M}^{-1} is not necessary and $\delta_{t+\Delta t}$ can be calculated by only matrix-vector multiplications in Equation (7). KOMATITSCH and TROMP (1999) performed exact diagonalization of the mass matrix using irregular spacing based on the Legendre polynomials, however we choose a piecewise regular spacing giving priority to easy mesh generation. Since the nodal coordinates of the elements can be easily calculated, they need not be memorized for our piecewise regular spacing.

Voxel Elements

In this section we will explain the structures of the matrices and how to calculate the recursive Equation (7) in the voxel FEM. For simplicity we will show only the details of a 2-D plain-strain model (P-SV model), although, the extension to a 3-D model is straightforward except for the complexity associated with the increase of dimension. Since the Earth is approximated well with a layered model, we may divide the medium into several domains and assume a regular distribution of voxels in each domain.

If a domain has only a single voxel element with an area of $\Delta x \Delta z$ and constant density and moduli, there are four nodes and the element displacement vector

$${}^e\delta = (\mathbf{u}^1, \mathbf{u}^2, \mathbf{u}^3, \mathbf{u}^4), \quad \mathbf{u}^k = (u_x^k, u_z^k). \quad (8)$$

The element version of \mathbf{B} in Equation (5) consists of four 3×2 submatrices as

$${}^e\mathbf{B} = (\mathbf{B}^1, \mathbf{B}^2, \mathbf{B}^3, \mathbf{B}^4) \quad (9)$$

and \mathbf{D} is a 3×3 matrix. Therefore, the element stiffness matrix has the form

$${}^e\mathbf{K} = (\mathbf{k}^{mn}), \quad \mathbf{k}^{mn} = \int_0^{\Delta x} \int_0^{\Delta z} (\mathbf{B}^m)^T \mathbf{D} \mathbf{B}^n dx dz. \quad (10)$$

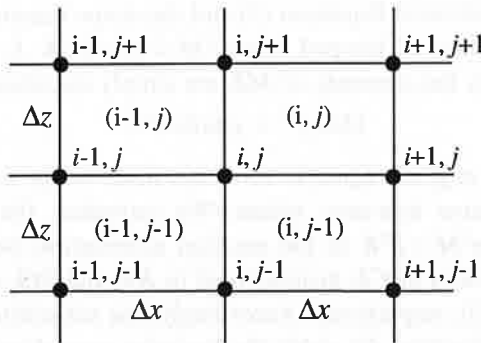


Figure 2
A target node and four voxel elements surrounding it.

The above definition guarantees the symmetry $k^{mn} = k^{nm}$ to eK . If the domain is isotropic and the shear strain is defined as $\gamma_{ij} = 2e_{ij} = \partial u_i / \partial x_j + \partial u_j / \partial x_i$, the modulus matrix D has the simple form

$$D = \begin{pmatrix} \lambda + 2\mu & \lambda & 0 \\ \lambda & \lambda + 2\mu & 0 \\ 0 & 0 & \mu \end{pmatrix}. \tag{11}$$

We now adopt the bi-linear Lagrange interpolation functions

$$N^1 = \frac{\Delta x - x}{\Delta x} \frac{\Delta z - z}{\Delta z}, \quad N^2 = \frac{x}{\Delta x} \frac{\Delta z - z}{\Delta z}, \quad N^3 = \frac{\Delta x - x}{\Delta x} \frac{z}{\Delta z}, \quad N^4 = \frac{x}{\Delta x} \frac{z}{\Delta z} \tag{12}$$

for the shape functions. These D and N make the whole eK symmetric, and k^{mn} is also symmetric or skew-symmetric. All the elements of eK are polynomials of $(\Delta z / \Delta x)^{\pm 1} (\lambda + 2\mu) / 6$, $\lambda / 4$ and $\mu / 4$. We can exploit these symmetry and simplicity of eK for an isotropic medium in order to reduce memory requirement and computation time of the voxel FEM simulation.

We next consider a domain with a $I \times J$ mesh. If the shape functions N^k are localized in a single element, the integral of the stiffness matrix K in Equation (5) can be partitioned as

$$K = \sum_{e=(1,1)}^{(I,J)} \int {}^eB^T D {}^eB dV. \tag{13}$$

We then assume the node (i, j) to be a target (Fig. 2). Since this node is shared by the four voxel elements surrounding it, the corresponding element of the vector $K\delta$ is given by the algebra

$$(K\delta)_i^{i,j} = {}^{(i-1,j-1)}k^{A1} u^{i-1,j-1} + {}^{(i-1,j)}k^{A2} + {}^{(i,j-1)}k^{B1} u^{i,j-1} + \dots \tag{14}$$

When a target node is located on the outer boundary of the domain, some of the surrounding elements and nodes are missing. In such a case, k^{mn} of a missing element and u^k of a missing node will be set to be zero.

Similarly, the definition in Equation (5) and the shape functions in Equation (12) yield the element matrix of lumped mass ${}^e\mathbf{M} = \rho\Delta x\Delta z/4 \cdot \mathbf{I}$, where \mathbf{I} is an 8×8 identity matrix, and so the elements of $\mathbf{M}\delta_t$ are simply calculated by

$$(\mathbf{M}\delta_t)^{ij} = \rho\Delta x\Delta z u^{ij}. \quad (15)$$

Most of the elements of f_t are equal to zero, but those at the nodes, to which body forces are applied, have non-zero values. We introduce the Rayleigh damping approximation ${}^e\mathbf{C} = \alpha{}^e\mathbf{M} + \beta{}^e\mathbf{K}$ to the medium attenuation (see *e.g.* CLOUGH and PENZIEN, 1975). The parts of $\mathbf{C}\delta_t$ proportional to $\mathbf{K}\delta_t$ and $\mathbf{M}\delta_t$ can be calculated by Equations (14) and (15), respectively. Accordingly, the substitution of Equation (15) for the first term of Equation (7) yields the recursive procedure

$$u_{t+\Delta t}^{ij} = 2u_t^{ij} - u_{t-\Delta t}^{ij} + \frac{(\Delta t)^2}{\rho\Delta x\Delta z} \left[f_t^{ij} - (\mathbf{K}\delta_t)^{ij} - \frac{1}{\Delta t} (\mathbf{C}(\delta_t - \delta_{t-\Delta t}))^{ij} \right], \quad (16)$$

where $(\mathbf{K}\delta_t)^{ij}$ will be given by Equation (14). We will calculate $(\mathbf{C}(\delta_t - \delta_{t-\Delta t}))^{ij}$ from Equations (14) and (15) replacing u_t^{ij} with $u_t^{ij} - u_{t-\Delta t}^{ij}$.

If we can assume constant density and moduli as well as regular spacing in a domain, the element matrices are common for all the finite elements of the domain and so we need memorize only representative matrices. This domain modeling will significantly reduce the memory requirement of the voxel FEM.

Accuracy

We have shown in the preceding sections that the Galerkin FEM discretization of the weak form of the governing equation (1) with a voxel mesh results in the recursive procedure of Equation (16). However, this equation looks too complicated and it is difficult to compare by sight its accuracy in space with that of FDM. Thus we extract $\partial u_x/\partial x$ and $\partial u_z/\partial x$ from $\partial \tau_{ij}/\partial x_j$ in Equation (1) and discretize it for the comparison with the second-order difference in space. Since the results for $\partial u_x/\partial x$ and $\partial u_z/\partial x$ will be identical, we represent u_x or u_z just with u in this section.

The weak form of $\partial u/\partial x$ and the linear shape functions (12) yield

$${}^e\mathbf{J}_x = (\mathbf{j}^{mn}), \quad \mathbf{j}^{mn} = \int_0^{\Delta x} \int_0^{\Delta z} N^m \frac{\partial N^n}{\partial x} dx dz, \quad (17)$$

where ${}^e\mathbf{J}_x$ is the part of ${}^e\mathbf{K}$ related to $\partial u/\partial x$. After similar algebra to Equations (10) and (14) we obtain

$$\begin{aligned} (\mathbf{J}_x\delta_t)^{ij} = & -\frac{\Delta z}{12} u^{i-1,j-1} + \frac{\Delta z}{12} u^{i+1,j-1} - \frac{\Delta z}{3} u^{i-1,j} \\ & + \frac{\Delta z}{3} u^{i+1,j} - \frac{\Delta z}{12} u^{i-1,j+1} + \frac{\Delta z}{12} u^{i+1,j+1}. \end{aligned} \quad (18)$$

The integration in Equation (17) implies that $\partial u/\partial x$ is averaged over a single element, and so $\partial u/\partial x$ is approximated with $(J_x \delta_i)^{i,j}$ divided by the element area $\Delta x \Delta z$. This approximation and the arrangement of the terms in Equation (18) lead to

$$\frac{\partial u}{\partial x} \sim \frac{1}{3} \left[2 \cdot \frac{1}{2\Delta x} (u^{i+1,j} - u^{i-1,j}) + 1 \cdot \frac{1}{2\Delta x} \left(\frac{u^{i+1,j+1} + u^{i+1,j-1}}{2} - \frac{u^{i-1,j+1} + u^{i-1,j-1}}{2} \right) \right]. \quad (19)$$

The first term of the above equation is identical to the second-order (three-point) difference operator of $\partial u/\partial x$ used in FDM. $u^{i+1,j}$ and $u^{i-1,j}$ in this term are the displacements at the two nodes neighboring the target (i,j) along the horizontal axis. Four displacements $u^{i+1,j+1}$, $u^{i+1,j-1}$, $u^{i-1,j+1}$ and $u^{i-1,j-1}$ are also given at the nodes distributed along the two neighboring axes. In the second term, the mean of $u^{i+1,j+1}$ and $u^{i+1,j-1}$ approximates $u^{i+1,j}$, and a similar mean approximates $u^{i-1,j}$. These means also form a second-order difference operator. Accordingly, the FEM operator of $\partial u/\partial x$ consists of the second-order FDM operator and its approximation calculated from the displacements at the nodes surrounding the target. They are averaged with a half weight to the latter, and the accuracy of the FEM operator is supplemented by additional accuracy from the latter. This additional accuracy will relax the condition of Δt for numerical stability as shown in the section '2-D verification.'

We now evaluate the truncation error in the FEM operator using Taylor expansion. The error of the second-order FDM operator is $O((\Delta x)^2)$ (e.g., KREYSZIG, 1999). The error of the second term in Equation (19) is estimated to be $O((\Delta x)^2, (\Delta z)^2)$ from the Taylor expansions of $u^{i+1,j+1} = u(x + \Delta x, z + \Delta z)$, $u^{i+1,j-1} = u(x + \Delta x, z - \Delta z)$, $u^{i-1,j+1} = u(x - \Delta x, z + \Delta z)$ and $u^{i-1,j-1} = u(x - \Delta x, z - \Delta z)$. Therefore, the FEM operator involves the truncation error of the same order as the second-order FDM operator, if we keep Δx and Δz on the same order. This implies that the FEM operator may cause numerical dispersion in a similar way to the FDM operator.

In the traditional FEM approach, tetrahedra are used to model a very complex structure as schematically shown in Figure 3a (e.g., BAO *et al.*, 1998). KOMATITSCH and VILOTTE (1998) adopted a mesh in curvilinear coordinates to model very complex underground structure and surface topography utilizing their layered features. However, only voxels are allowed in our voxel FEM, so that discretization errors of the same order as FDM may be introduced. To avoid these problems we have to use a finer submesh for any complex part of the model. The submesh interval should be smaller than in the tetrahedron mesh as shown in Figure 3b.

We have built the equation of motion in the weak form (2) imposing the traction-free condition on the outer boundary of the medium. Therefore the free-surface condition at the upper part of the boundary is automatically satisfied, even though it

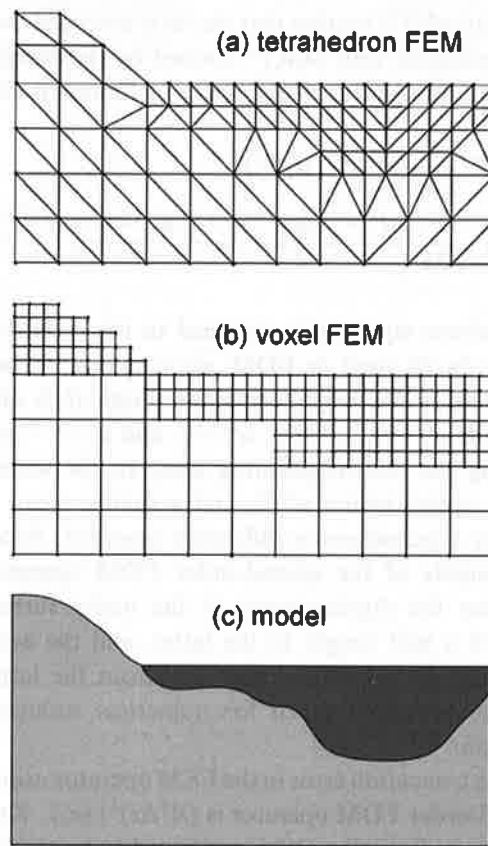


Figure 3

(a) Tetrahedron and (b) voxel meshes for the underground structure in (c).

has arbitrary shape. This is one of the greatest advantages of FEM over FDM. However, the side and lower parts of the boundary may cause artificial reflections if we do not apply a suitable boundary condition in addition to the traction-free condition. We introduce here the viscous boundary condition of LYSMER and KUHLMAYER (1975) to avoid this difficulty. A buffer zone of 10 ~ 20 elements in width is also defined adjacently to the side and lower parts, and we assign large damping moduli there to further attenuate artificial reflections.

2-D verification

For numerical examples of the voxel FEM, we first compute seismograms from an explosive line source buried in a 2-D fullspace of $V_P = 6.0$ km/s, $V_S = 3.0$ km/s, $\rho = 2.5$ km/s

and $Q_p = 40$. To simulate the fullspace the buffer zone is also defined along the upper boundary of a halfspace in addition to the side and lower boundaries. The right panel of Figure 4 shows the displacements of nodes at the same level as the source. They favorably compare with the seismograms computed by FDM and semi-analytical solutions by the discrete wavenumber (DW) method (TAKENAKA, 1990) in the middle and left panels.

We can find slight differences in the tails of the P-wave pulses when we carefully inspect the seismograms at distances further than 30 km. They arise from the difference in the implementation of medium attenuation. While the frequency-independent Q model is built in the DW method, it is approximated with the damping matrix proportional to the mass matrix. The approximation, which is equivalent to the constant damping coefficient in the equation of motion for FDM, results in the slight distortion of the remote FEM and FDM seismograms. We can incorporate a more accurate attenuation model (e.g., CARCIONE *et al.*, 1988), but this will significantly increase memory requirement and computation time.

It takes 54 s for the voxel FEM on a 2.0 GHz Pentium to complete the 1000-step time history in a 512×256 mesh using 3.8 MB memory, while FDM of FURUMURA and TAKENAKA (1995) spends 46 s computational time for the same

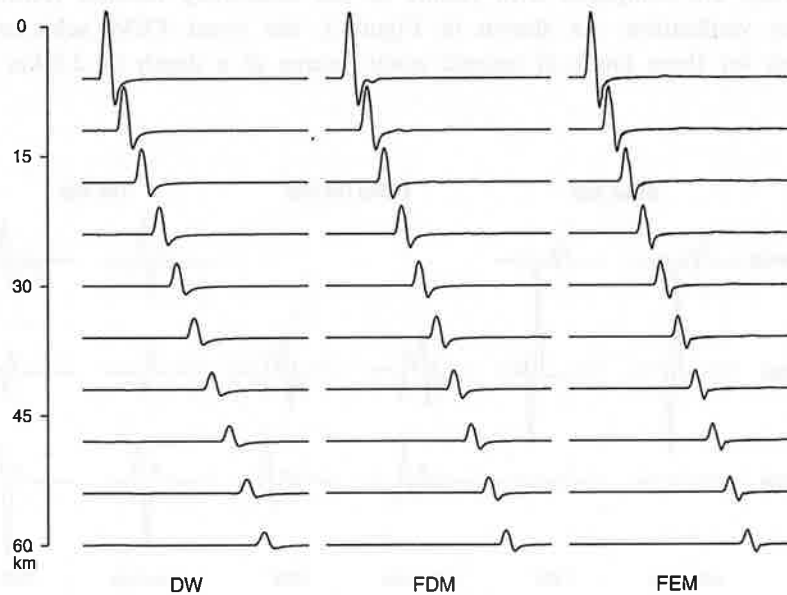


Figure 4

Comparison of seismogram sections simulated by the discrete wavenumber method (left), FDM (middle) and FEM (right).

configuration using 3.7 MB memory. In other words, the voxel FEM runs 85% as fast as FDM using a similar amount of computer memory to that of FDM. This memory requirement is for a case of the domain modeling mentioned in the section 'Voxel elements.' The FEM code includes ten reserved domains, two of which were used for the medium and buffer zone. If we do not use the domain modeling, we have to allocate five times larger memory.

A time step Δt longer than 0.10 s leads to numerical instability in the recursive procedure (16) for the above example. Using the Courant condition

$$\Delta t < c \frac{\min(\Delta x, \Delta z)}{V_P} \quad (20)$$

for the P-wave propagation, we interpret $\Delta t < 0.10$ s as the Courant number $c = 0.80$. On the other hand, The FDM calculation becomes unstable for $\Delta t > 0.056$, and so c of FDM is 0.45. Therefore, the additional accuracy of Equation (19) relaxes the Courant condition allowing a time step 1.8 times longer than in FDM.

3-D verification

We also calculate ground motions from a point source in a 3-D half space ($V_P = 4.0$ km/s, $V_S = 2.3$ km/s, $\rho = 1.8$ g/cm³) of GRAVES (1996) using the voxel FEM. They are compared with results of the reflectivity method (KOHKETSU, 1985) for verification. As shown in Figure 5, the voxel FEM achieves good agreement for three kinds of seismic point source at a depth of 2.5 km in the

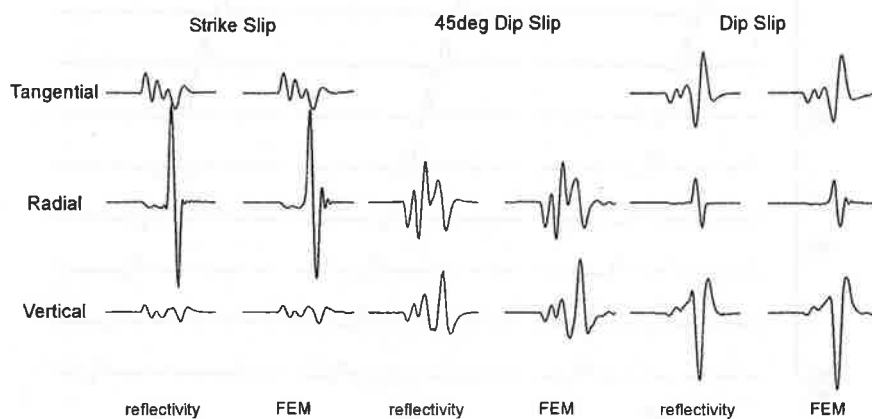


Figure 5

Ground motions due to a point source in the halfspace of GRAVES (1996) (left: reflectivity method, right: FEM).

halfspace with a cosine time function 1 s long. It takes 1.4 hour for the voxel FEM to complete the 20 s (800 steps; 0.025 s interval) time history of a $30 \times 30 \times 10$ km medium (4,608,000 elements; 125 m interval) on a 1.7 GHz Pentium, while FDM of FURUMURA *et al.* (2000) spends 1.0 hour for the same configuration. The voxel FEM requires a similar amount of memory to that of FDM. The next verification is carried out for a strike slip source at a depth of 1.6 km in a horizontally layered structure. This three-layer model was also proposed by GRAVES (1996). The FEM code occupies 675 MB memory for 12,800,000 elements, and again achieves good agreement as shown in Figure 6.

As mentioned earlier, the greatest advantage of FEM is that the traction-free condition has already been cast in the formulation. No special treatment is needed for a free surface with arbitrary shape. In order to confirm this advantage, another test of GRAVES (1996) is carried out in the halfspace. The dashed FK seismograms in Figure 7 should be correct. Although the FDM results somewhat fail to agree with them, the results by the voxel FEM achieve good agreement.

To describe how to deal with a piecewise regular mesh, we again adopt the above three-layer model and compute tangential seismograms. A fine submesh with intervals of 37.5 m is introduced into the shallow part of the model. Coarse spacing of 75 m is applied to the other part of the piecewise regular mesh as in the regular mesh. The computation in each submesh is carried out independently, and then displacements and velocities on both sides of a submesh boundary are averaged with weights of lumped masses at common nodes as shown in the right diagram of Figure 8. These averages will be used at the nodes in the next time step. The seismogram in the regular mesh fairly agrees with that by the reflectivity method, and the agreement is improved in the piecewise regular mesh as shown in the left and middle panels, since the fine submesh minimizes numerical dispersion in the low-velocity portion of the model.

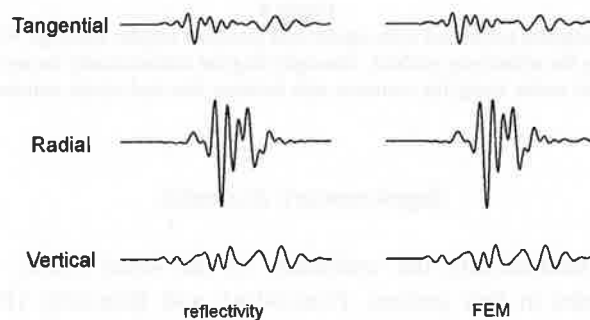


Figure 6

Ground motions due to a point source in the layered structure of GRAVES (1996) (left: reflectivity method, right: FEM).

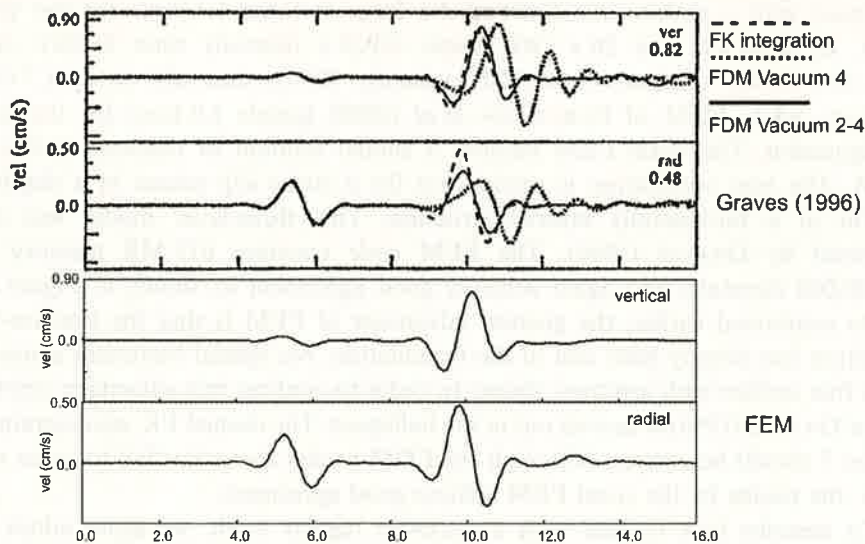


Figure 7

Comparison of seismograms calculated with the FK technique, the FDM using the modified vacuum formulations (after GRAVES, 1996), and the voxel FEM.

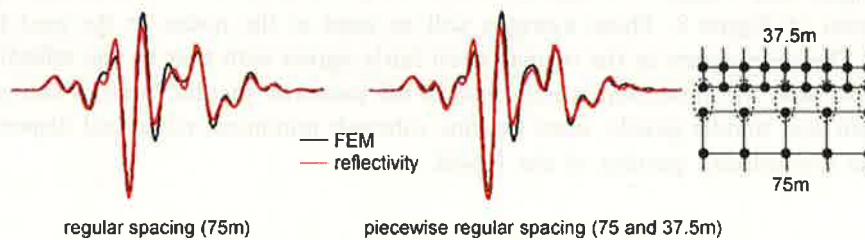


Figure 8

Comparison of seismograms calculated with regular and piecewise regular spacings. We also compare them to the seismogram by the reflectivity method. The right diagram schematically shows how to deal with the special nodes along the common side between fine and coarse submeshes.

Supplementary Examples

In order to demonstrate the usefulness of the voxel FEM, we show some numerical examples in this section. FURUMURA and KOKETSU (1998) performed FDM simulations in three typical geological settings, which are an exposed bedrock, flat sediments and a sedimentary basin shown in Figure 9. Their resultant peak ground velocity distributions are presented in the three panels on the left-hand side.

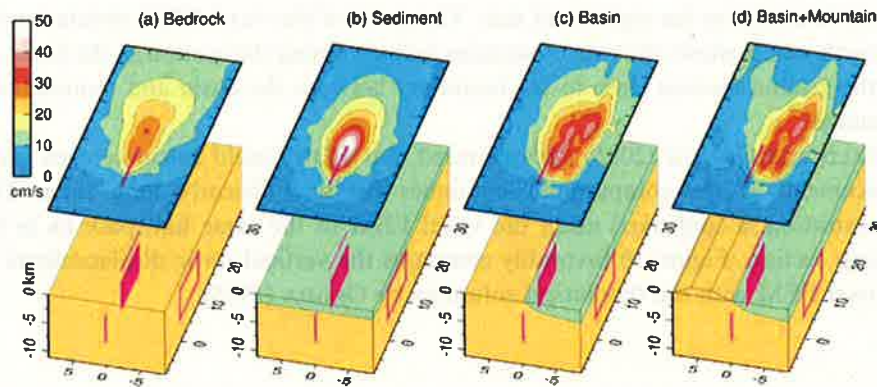


Figure 9

Peak ground velocity distributions due to a 10 by 5 km strike slip fault ($M6$) at a depth of 2 km buried in (a) an exposed bedrock, (b) flat sediments, (c) a sedimentary basin and (d) a basin neighboring the mountain range.

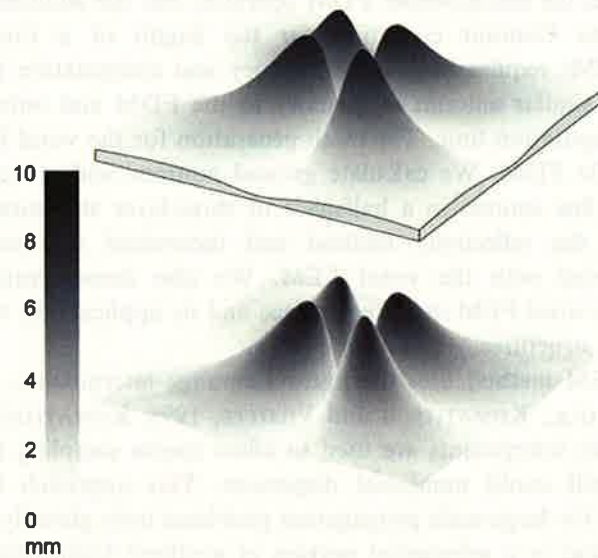


Figure 10

Distribution of vertical static displacements due to a strike slip in the half space (upper: OKADA'S (1985) solution, lower: FEM).

The basin model is constructed based on the geology around the area damaged by the 1995 Kobe earthquake, however the surface topography in a mountain range neighboring the sedimentary basin is neglected because of the limitations of FDM. Since FEM requires no special treatment for including the topography, we construct

the fourth model on the right hand side. The result of the voxel FEM simulation for the fourth model shows that the mountains look confining the motion of the basin, so that the ground motion close to the boundary between the basin and mountains is attenuated.

WALD and GRAVES (2001) demonstrated that FDM could calculate even static displacements if the computation continues for a sufficiently long time. This demonstration is confirmed using the voxel FEM in the same halfspace as in the previous section. Figure 10 favorably compares the vertical static displacements by the voxel FEM with the theoretical solutions by OKADA (1985).

Conclusions and Discussion

The FEM has been reformulated for seismic ground motion simulation using a voxel mesh and its accuracy is assessed with a discrete representation of the spatial derivative $\partial u/\partial x$. The voxel FEM operator involves a truncation error of the same order as the second-order FDM operator, but the additional accuracy of FEM relaxes the Courant condition for the length of a time step. While conventional FEMs require both large memory and computation time, the voxel FEM requires a similar amount of memory to the FDM and only takes 1.2~1.4 times longer computation time. The mesh generation for the voxel FEM is as easy and fast as in the FDM. We calculate ground motions and static displacements due to point or line sources in a halfspace or three-layer structure. Comparisons with results of the reflectivity method and theoretical solutions show good agreement achieved with the voxel FEM. We also demonstrate the inherent advantage of the voxel FEM at a free surface and its applicability to complex 3-D topography and structures.

The voxel FEM method uses the linear Lagrange interpolants. In the spectral element method (*e.g.*, KOMATITSCH and VILOTTE, 1998; KOMATITSCH and TROMP, 1999) higher-order interpolants are used to allow coarse sampling by the medium elements, and still avoid numerical dispersion. This approach has been very successfully used for large-scale propagation problems both globally (CHALJUB and VILOTTE, 1998) and in a substantial portion of southern California (KOMATITSCH *et al.*, 2002). However, for the class of shallow structure which need to be represented for studies of seismic ground motion, the variations in medium properties can be so fast that small cells are essential. Frequently the sampling will need to be so fine that it would be very difficult to adopt the meshes employed in the spectral element method. The simple voxel FEM approach can be used with several scales of cells to provide an effective scheme for simulating seismic ground motion even with rapid variations in a near-surface structure.

Acknowledgements

This research was supported by the Japan Science and Technology Corporation under the ACT-JST program 13C-2. We greatly appreciate Brian Kennett (ANU) for his careful reviews. Hiroshi Takenaka (Kyushu Univ.) kindly provided us with 2-D discrete wavenumber codes. Comments by J. P. Vilotte (IPGP) and the anonymous reviewer are very helpful in improving the manuscript. Some parts of Figures 9 and 10 were drawn by GMT of Drs. Wessel and Smith.

REFERENCES

- BAO, H., BIELAK, J., GHATTAS, O., KALLIVOKAS, L. F., O'HALLARON, D. R., SHEWCHUK, J. R., and XU, J. (1998), *Large-scale Simulation of Elastic Wave Propagation in Heterogeneous Media on Parallel Computers*, *Comput. Meth. Appl. Mech. Eng.* 152, 85–102.
- CARCIONE, J. M., KOSLOFF, D., and KOSROFF, R. (1988), *Wave Propagation Simulation in a Linear Viscoelastic Medium*, *Geophys. J.* 95, 597–611.
- CHALJUB, E. and Vilotte, J. P. (1998), *3-D Wave Propagation in a Spherical Earth Model Using the Spectral Element Method*, *EOS (Trans. Am. Geophys. Un.)* 79, 625–626.
- CLOUGH, R. W. and PENZIEN, J. (1975), *Dynamics of Structures* (McGraw-Hill, New York).
- FURUMURA, T., KENNETT, B. L. N., and TAKENAKA, H. (1998), *Parallel 3-D Pseudospectral Simulation of Seismic Wave Propagation*, *Geophys. J.* 63, 279–288.
- FURUMURA, T. and KOKETSU, K. (1998), *Specific Distribution of Ground Motion during the 1995 Kobe Earthquake and its Generation Mechanism*, *Geophys. Res. Lett.* 25, 785–788.
- FURUMURA, T., KOKETSU, K., and TAKENAKA, H. (2000), *A Hybrid PSM/FDM Parallel Simulation for Large-scale 3-D Seismic (acoustic) Wavefield*, *Geophys. Explor.* 53, 294–308.
- FURUMURA, T. and TAKENAKA, H. (1995), *2.5-D Modeling of Elastic Waves Using the Pseudospectral Method*, *Geophys. J. Int.* 124, 820–832.
- GRAVES, R. W. (1996), *Simulating Seismic Wave Propagation in 3-D Elastic Media Using Staggered Grid Finite Differences*, *Bull. Seismol. Soc. Am.* 86, 1091–1106.
- KOKETSU, K. (1985), *The Extended Reflectivity Method for Synthetic Near-field Seismograms*, *J. Phys. Earth* 33, 121–131.
- KOMATITSCH, D. and TROMP, J. (1999), *Introduction to the Spectral Element Method for Three-dimensional Seismic Wave Propagation*, *Geophys. J. Int.* 139, 806–822.
- KOMATITSCH, D., TROMP, J., SHAW, J., SUESS, P., and STIDAM, C. (2002), *Simulations of Strong Ground Motion in the Los Angeles Basin Using the Spectral-Element Method*, *EOS, (Trans. Am. Geophys. Un.)* 83, Fall Meet. Suppl., Abstract S51C-02.
- KOMATITSCH, D. and VILLOTTE, J.-P. (1998), *The Spectral Element Method: An Efficient Tool to Simulate the Seismic Response of 2-D and 3-D Geological Structures*, *Bull. Seismol. Soc. Am.* 88, 368–392.
- KREYSZIG, E. (1999), *Advanced Engineering Mathematics* (John Wiley & Sons, New York), 8-th edition.
- LYSMER, J. and KUHLMEYER, R. L. (1975), *Finite Dynamic Model for Infinite Media*, *J. Eng. Mech. Div., ASCE.* 95, 859–877.
- OKADA, Y. (1985), *Surface Deformation due to Shear and Tensile Faults in a Half-space*, *Bull. Seismol. Soc. Am.* 75, 1135–1154.
- OLSEN, K. B., ARCHULETA, R. J., and MATARESE, J. R. (1995), *Three-dimensional Simulation of a Magnitude 7.75 Earthquake on the San Andreas Fault*, *Science*, 270, 1628–1632.
- TAKENAKA, H. (1990), *Theoretical Studies on Seismic Wave Fields in Irregularly Layered Media*, Ph.D. Thesis, Hokkaido University, Sapporo.
- TOP500 (1994), *TOP500 List for November 1994*, <http://www.top500.org/dlist/1994/11/>.
- UDIAS, A. (1999), *Principles of Seismology* (Cambridge University Press, Cambridge).

VAN RIETBERGEN, B., WEINANS, H., HUISKES, R., and POLMAN, B. J. W. (1996), *Computational Strategies for Iterative Solutions of Large FEM Applications Employing Voxel Data*, *Int. J. Num. Met. Eng.* **39**, 2743–2767.

WALD, D. J. and GRAVES, R. W. (2001), *Resolution Analysis of Finite Fault Source Inversion using one- and Three-dimensional Green's Functions 2. Combining Seismic and Geodetic Data*, *J. Geophys. Res.* **106**, 8767–8788.

(Received September 27, 2002, revised February 28, 2003, accepted March 7, 2003)



To access this journal online:
<http://www.birkhauser.ch>
